Supporting Information:

Full electrical control of multiple resistance states in van der Waals sliding multiferroic tunnel junctions

Jie Yang,[1, 2] Baochun Wu,[2] Jun Zhou,[3] Jing Lu,[2, 4, 5, 6 †] Jinbo Yang,[2, 4, 5, 6, ‡] and Lei Shen[7, *]

[1] Key Laboratory of Material Physics, School of Physics and Microelectronics, Ministry of Education, Zhengzhou University, Zhengzhou 450001, P. R. China
[2] State Key Laboratory for Artificial Microstructure and Mesoscopic Physics and School of Physics, Peking University, Beijing 100871, P. R. China
[3] Institute of Materials Research & Engineering, A*STAR (Agency for Science, Technology and Research), 2 Fusionopolis Way, Innovis, Singapore 138634, Singapore
[4] Collaborative Innovation Center of Quantum Matter, Beijing 100871, P. R. China
[5] Beijing Key Laboratory for Magnetoelectric Materials and Devices (BKL-MEMD), Peking University, Beijing 100871, P. R. China
[6] Yangtze Delta Institute of Optoelectronics, Peking University, Nantong 226010 Jiangsu, P. R. China
[7] Department of Mechanical Engineering, National University of Singapore, 9 Engineering Drive 1, Singapore 117575, Singapore

Email: [†]jinglu@pku.edu.cn; [‡]jbyang@pku.edu.cn; [*]shenlei@nus.edu.sg

Table of Contents

1. Geometric and electronic properties of BBN, CrI_3, $MnBi_2Te_4$, and $CrI_3|MnBi_2Te_4$

We start by revealing the electronic properties of the atomically thin BBN, CrI_3, and $MnBi_2Te_4$, the framework of the vdW MFTJs. In the AB- (BA-) stack BBN (Fig.S1a), the more electronegative N atoms in the interlayer N-B pairs distort the $2p_z$ orbital, generating vertical electric dipoles.[1-2] The AB and BA stacking orders as well as the polarization direction can be switched by sliding one-third of their unit cells. The magnetic moments in CrI_3 are aligned along the out-of-plane direction by I^- ion-mediated Cr-Cr exchange coupling (Fig. S1b).[3] The calculated bandgaps of the FM 1L CrI_3 are 0.91 eV (3.01 eV) for the spin up (spin down) and 1.00 eV for spin-orbit coupling (SOC) (Figs. S1c and f). The AFM exchange coupling of bilayer CrI_3 is 2.13 meV (2.34 meV) per unit cell without (with) SOC (Table S1). Multilayer $MnBi_2Te_4$ has intrinsic A-type out-of-plane AFM order. The AFM exchange coupling for two-septuple layer (2-SL) $MnBi_2Te_4$ is calculated as 8.50 eV (6.26 eV) in $\sqrt{3} \times \sqrt{3}$ supercell without (with) SOC (Table S1). Whereas the 1-SL $MnBi_2Te_4$ is a FM semiconductor with a calculated bandgap of 0.93 eV (1.18 eV) for the spin up (spin down) channel, and 0.24 eV after considering SOC (Figs. S1d and g).[4-5]

The heterostructure of 1L CrI_3 on 1-SL $MnBi_2Te_4$ forms very strong FM coupling. The CrI_3-MBT heterostructure in Fig. S1b is made up of a unit cell of 1L CrI_3 and a $\sqrt{3} \times \sqrt{3}$ supercell of 1-SL $MnBi_2Te_4$ with a mismatch of 7%.[5] The optimized interlayer distance is 2.96 Å. The energy difference ΔE between the FM and AFM orders of CrI_3-MBT is -35.84 meV, which is consistent with previous results.[5] Such strong FM pining is larger than the interlayer exchange coupling of bilayer CrI_3 (2.13 meV) and 2-SL $MnBi_2Te_4$ (8.50 meV) with the same lattice dimension used in the heterostructure. This FM pinning strength is barely affected by the SOC (ΔE =-34.18 meV).

Notably, the 100% spin-polarized conduction bands around 0.6 eV (Fig. S1c) in the 1L CrI_3 are downwards shifted to (around) the Fermi level in Fig. S1e (h), exhibiting a half-metallic feature after contacting with the 1-SL $MnBi_2Te_4$. The half-metallic character implies a high spin screening efficiency and thus a high TMR performance when made into devices. The half-metallicity of the 1L CrI_3 is caused by the electron drift from the higher Fermi level of 1-SL $MnBi_2Te_4$(work function W_f =5.65 eV) to the lower one of 1L CrI_3 (W_f =8.22 eV) after contacting. The W_f of the CrI_3-MBT heterostructure is 5.77 eV, very close to that of the 1-SL $MnBi_2Te_4$. This band alignment is again verified in MFTJs transport calculations, which are discussed in main text.

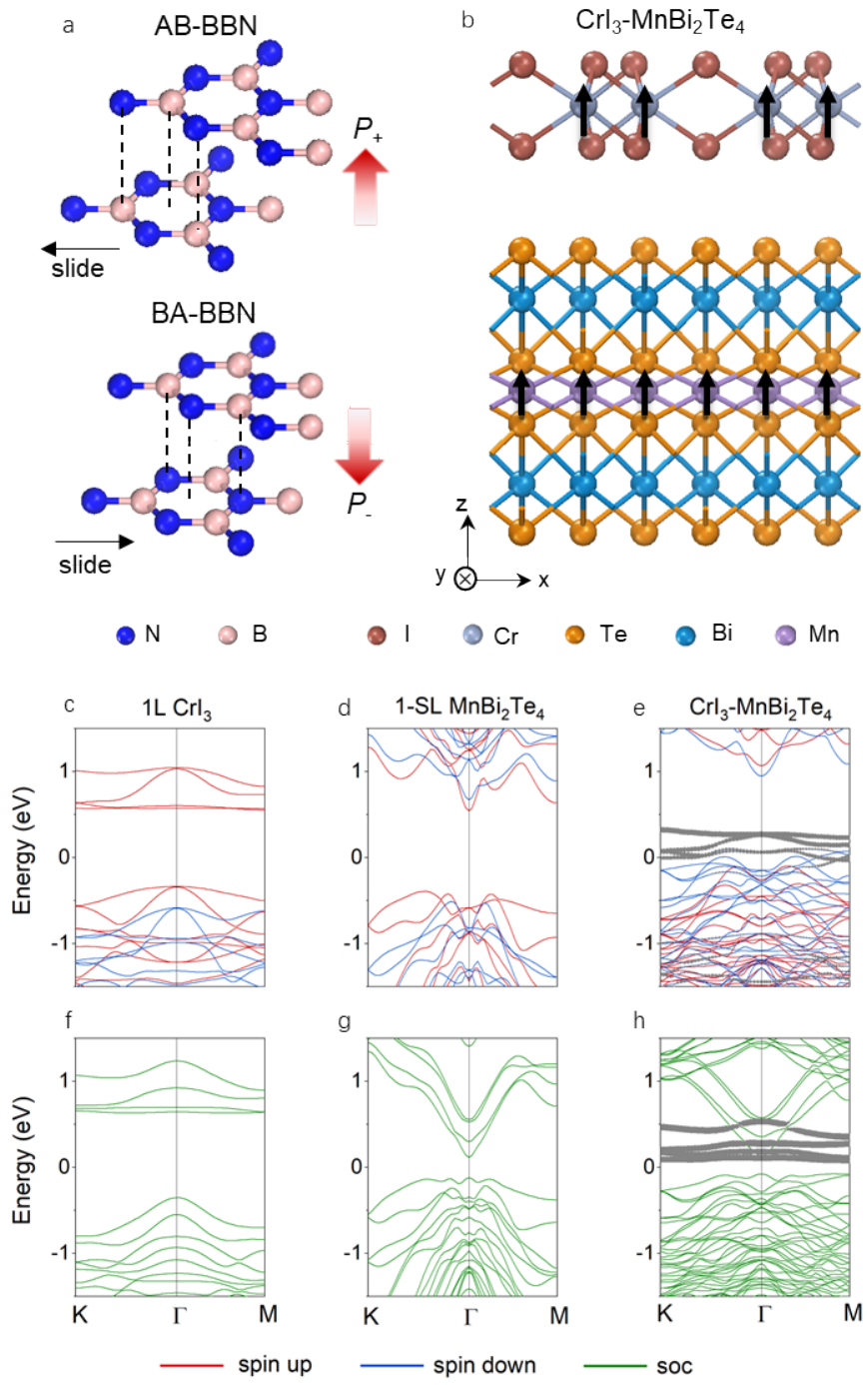

Fig. S1 Geometric and electronic structures of 2D ferroics materials in MFTJs. (a) Atomic arrangement of AB- and BA-stack bilayer *h*-BN (BBN). Ferroelectric polarization is labeled by the upward or downward red arrow. Sliding along the black arrow direction switches the ferroelectricity. (b) Side atomic view and ground magnetic state (black arrows) of the CrI_3-$MnBi_2Te_4$ (CrI_3-MBT) heterostructure. Spin-resolved band structures for 1 L CrI_3, 1-SL $MnBi_2Te_4$, and CrI_3-MBT heterostructure are shown in (c-e), respectively. (f-h) The same with (c-e) but includes spin-orbit coupling. The gray dots in (e) and (h) are projected Cr atoms. The Fermi level is set to zero.

Table S1 Total energy difference ΔE between the ferromagnetic and antiferromagnetic configurations for bilayer (BL) CrI_3, 2-SL $MnBi_2Te_4$, and the interface of monolayer CrI_3 on 1-SL $MnBi_2Te_4$. Results with and without spin-orbit coupling (SOC) are shown.

		BL CrI_3 (1×1)	2-SL $MnBi_2Te_4$ $(\sqrt{3}\times\sqrt{3})$	CrI_3-$MnBi_2Te_4$ (1×1)/$(\sqrt{3}\times\sqrt{3})$
$\Delta E=E_{FM}-E_{AFM}$ (meV)	w/o SOC	2.13	8.50	-35.84
	SOC	2.34	6.26	-34.18

2. Ferroelectricity of the whole device

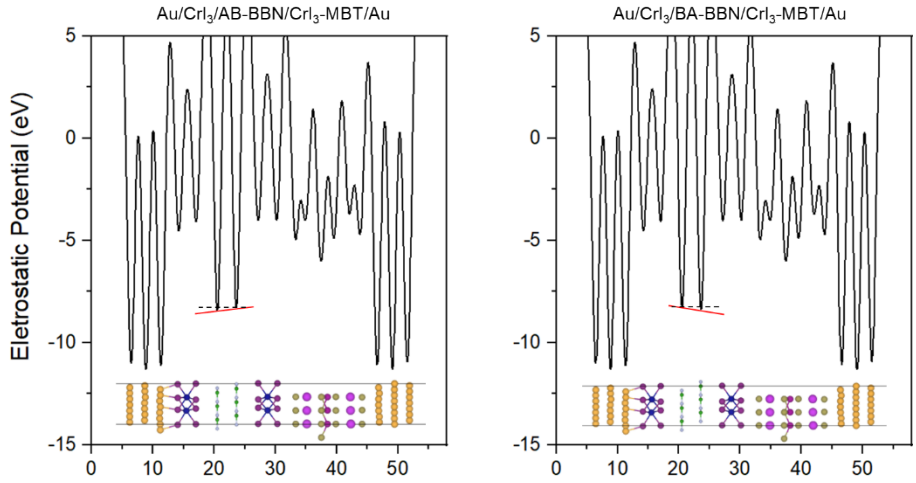

Fig. S2 Planar averaged electrostatic potential of Au/CrI_3/BBN/CrI_3-$MnBi_2Te_4$/Au with AB- and BA-stacked configurations of BBN. The red lines connect the potentials of two BN layers.

Theoretically, once the energy provided by the electric field exceeds the sliding barrier (0.6 eV) based on our calculation, the polarization of BBN would be reversed. We can not directly calculate the specific threshold voltage that induces the BBN to finish sliding. Therefore, we make a rough approximation using the formula of energy density ω of the statistic electric field E:

$$\omega = \frac{\varepsilon_0}{2} E^2 ,$$

where ε_0, the vacuum dielectric constant, is 8.85×10^{-12} F/m. In our MFTJ, $\omega = \frac{0.6\ \text{eV} \times 1.6 \times 10^{-19}}{7.55\ \text{nm} \times 7.55\ \text{nm} \times 5\ \text{nm}} = 0.34 \times 10^{9}\ \text{J/m}^3$, and the electric field $\boldsymbol{E}$ is then given by 0.8 V/nm. This approximation strongly relies on the calculated device size. In this regard, we believe that referring to the experimental polarization-switching electric field is more convincing.

3. Spin-resolved device LDOS

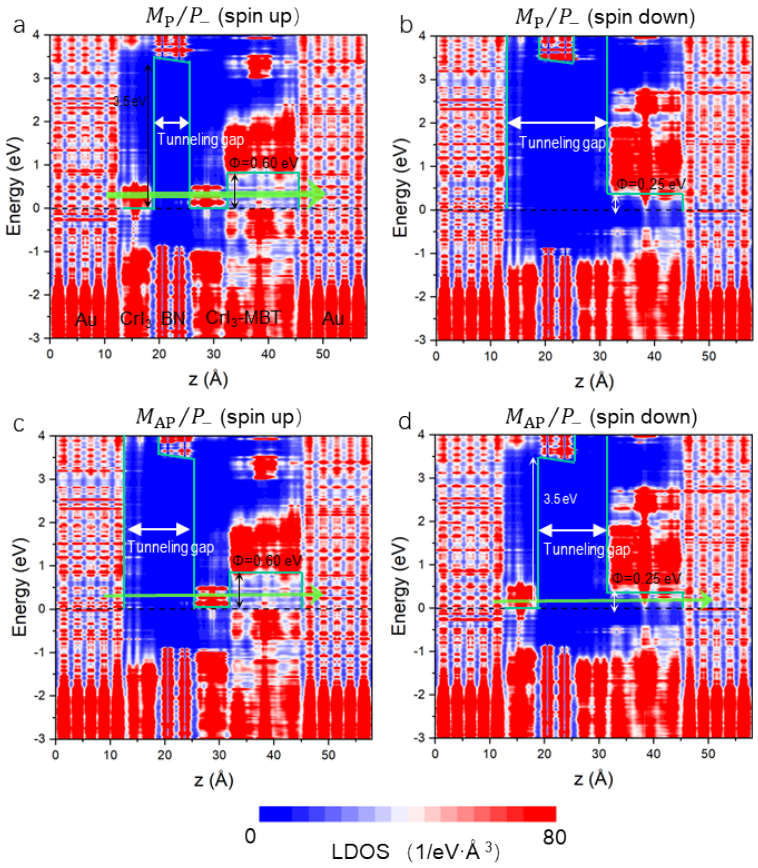

Fig. S3 Spin-resolved local density of states (LDOS) of the Au/CrI_3/**BA**-BBN/CrI_3-$MnBi_2Te_4$/Au MFTJ with the (a-b) parallel magnetization alignment of two CrI_3 layers and (c-d) the antiparallel alignment. Two vertical green lines profile tunneling barriers. Green arrows indicate the tunneling direction in the device. The Fermi level refers to zero, marked by black dashed lines.

4. Transmission spectra of MFTJs under different bias voltages

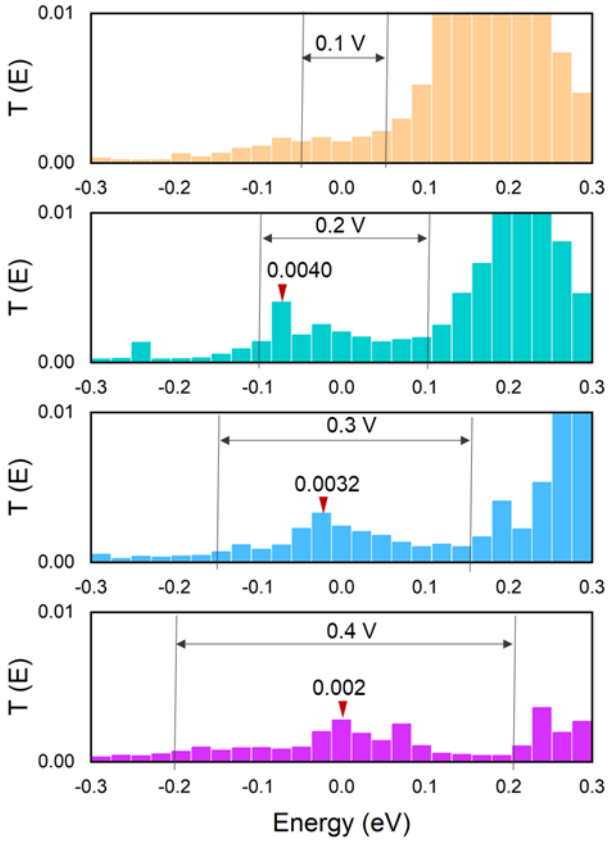

Fig. S4 Transmission spectra of the Au/CrI_3/**AB**-BBN/CrI_3-$MnBi_2Te_4$/Au MFTJs under bias of 0.1, 0.2, 0.3, and 0.4 V, respectively, in the M_P state. Red triangles mark the main contribution to the current within the bias window.

5. Parameters for spin transfer torque calculations

Table S2 Summary of the theoretical parameters for spin transfer torque calculation in the Au/CrI_3/BBN/CrI_3-$MnBi_2Te_4$/Au MFTJ. α is the Gilbert damping factor, E_{MAE} the magnetic anisotropy energy, S the sectional area of the device, $T_{stt\text{-}z}$ the z component of spin transfer torque, V_c critical voltage for magnetization reversal, G the conductance, I_c the critical current for magnetization. All these parameters are obtained when the angle (θ) between two magnetic moments in the free and the pinned layers is 90°.

α	E_{MAE} (meV)	S (Å^2)	$T_{stt\text{-}z}$ (eV/V)	V_c (V)	G (e^2/h)	I_c (10^{10}A/m^2)
0.01	3.60	49.39	1.71×10^{-4}	0.21	9.27×10^{-4}	1.53

6. Outputs with SOC included under 0.4 V bias voltages

Table S3 The calculated current, TMR, and TER of the MFTJs at 0.4 voltage ($V_b = 0.4\,V$) with SOC.

V_b (V)		M_P state (↑↑)	M_{AP} state (↑↓)	**TMR**
0.4	I_{P+} (AB-BBN) (A)	4.1×10^{-8}	5.5×10^{-9}	640%
	I_{P-} (BA-BBN) (A)	3.7×10^{-8}	4.3×10^{-9}	749%
	TER	11%	26%	

7. References

1. Yasuda, K.; Wang, X.; Watanabe, K.; Taniguchi, T.; Jarillo-Herrero, P., Stacking-engineered ferroelectricity in bilayer boron nitride. *Science* **2021,** *372* (6549), 1458.

2. Vizner Stern, M.; Waschitz, Y.; Cao, W.; Nevo, I.; Watanabe, K.; Taniguchi, T.; Sela, E.; Urbakh, M.; Hod, O.; Ben Shalom, M., Interfacial ferroelectricity by van der Waals sliding. *Science* **2021,** *372* (6549), 1462.

3. Jiang, S.; Li, L.; Wang, Z.; Mak, K. F.; Shan, J., Controlling magnetism in 2D CrI_3 by electrostatic doping. *Nat. Nanotechnol.* **2018,** *13* (7), 549-553.

4. Li, J.; Li, Y.; Du, S.; Wang, Z.; Gu, B.-L.; Zhang, S.-C.; He, K.; Duan, W.; Xu, Y., Intrinsic magnetic topological insulators in van der Waals layered $MnBi_2Te_4$-family materials. *Sci. Adv.* **2019,** *5* (6), eaaw5685.

5. Fu, H.; Liu, C.-X.; Yan, B., Exchange bias and quantum anomalous Hall effect in the $MnBi_2Te_4/CrI_3$ heterostructure. *Sci. Adv.* **2020,** *6* (10), eaaz0948.